Evaluation of robustness against external vibrations for long-range MEMS lidar with one-dimensional resonant micromirror

Han Woong Yoo,[a,*] **David Brunner**,[a,b] **Matthias Macho**,[a] **Leonhard Niedermueller**,[b] **Angel Jurado Devesa**,[b] **Leonhard Kormann**,[b] **and Georg Schitter**[a]

[a]TU Wien, Automation and Control Institute (ACIN), Vienna, Austria
[b]Infineon Technologies Austria AG, Graz, Austria

Abstract. We describe the verification of a long-range one-dimensional (1D) scanning micro-electro-mechanical systems (MEMS) lidar specifically considering the robustness against external vibration influences. The 1D scanning MEMS lidar exploits a multichannel horizontal line laser to scan the scene vertically for a 10 deg × 11 deg horizontal and vertical field of view at a frame rate of up to 29 Hz. To evaluate the robustness against vibrations, a vibration evaluation setup is developed to apply a wideband vibration based on the automotive standard LV124. The vibration tests are performed in three conditions open loop without control and two phase-locked loops (PLLs) with default and high gain settings. The test results demonstrate that vibration can cause wobbly distortion along the scan angle in the open loop case and the PLLs can suppress effectively this influence in the mean and standard deviation of the standard point to surface error up to 69.3% and 90.0%, respectively. This verifies the benefits of the MEMS mirror control, ensuring stable point cloud measurements under vibrations in harsh automotive environments. [DOI: 10.1117/1.JOM.2.1.011007]

Keywords: MEMS; lidar; automotive; vibration; robustness.

Paper 21024SS received Nov. 22, 2021; accepted for publication Mar. 1, 2022; published online Mar. 23, 2022.

1 Introduction

Advancements of sensor technologies and artificial intelligence are about to bring a revolutionary change in mobility and transportation by autonomous driving.[1] Lidar is regarded as one of the key sensor technologies that enable a reliable perception of surroundings, especially providing high-resolution and long-distance 3D object detection in various road situations,[2] for example, a dropped black tire on a highway at over 100 m away.[3] To be adopted in most vehicles as standard safety equipment akin to airbags, the unit price of the lidar has to be reduced significantly while its reliability and the lidar lifetime should be improved like the entire car lifetime, which requires fundamental changes in the lidar design and its main components. For high resolution and long-range lidars, beam scanning systems are essential to deliver sufficient laser power to the scene while maintaining eye safety.[4]

Scanning mirrors based on micro-electro-mechanical systems (MEMS) technologies are one of the promising solutions for long-range scanning lidars,[5–14] thanks to a small form factor, high scanning frequencies with a wide field of view (FoV), long lifetime, and competitive unit cost in mass production. By scanning methods, the MEMS scanning lidars can be categorized in omniscan,[6] raster scan,[5,8,11] Lissajous scan,[14] and 1D line scan.[3,4,9] Compared with the other scanning methods, 1D scan lidar is a hybrid of the flash lidar and 2D point scanning lidar, allowing a high frame rate with fewer numbers of laser pulses and less complexity in sensor readout. However, the generation of a uniform laser line is not trivial with commercially available laser arrays. In addition, high laser power is still required due to the broadening of the laser into a line along one

*Address all correspondence to Han W. Yoo, yoo@acin.tuwien.ac.at

axis. This limits the detection range since the light sources must comply with class 1 laser specifications.

Moreover, MEMS scanning systems for use in automotive applications have to be highly robust against harsh environmental conditions such as vibrations, shocks, and temperature variations.[14,15] The vibration and shock influence on MEMS scanning mirrors has been investigated for electrostatic actuation,[11,16–18] electromagnetic actuation,[19] and piezoelectric actuation.[20] Vibration influences during scanning operations are evaluated in Refs. 16–19, where considerable performance improvements by the designed controllers have been shown. For a parametrically driven resonant MEMS mirror with a reinforcement structure, a large vibration influence is observed by translational vibrations along the direction of the scanning and in the vicinity of the mirror frequency.[16] This observation suggests to design the resonance frequency above 2 kHz considering the vibration spectrum profile of the automotive standard, e.g., LV124,[21] which does not specify broad-band vibration criteria above this threshold. A phase-locked loop (PLL) used for controlling the mirror also shows improved robustness against vibration by reducing the peak errors to its half and the robustness also depends on the gain choice of the PLL.[16,17] A more detailed analysis of the dynamics is discussed for time normalized PI PLL design in Ref. 22. The evaluation of MEMS scanning lidar measurements under external vibrations, however, has not been reported so far.

The main contribution of this paper is the evaluation of vibration influences in point cloud measurements of a long-range 1D scanning MEMS lidar. The used long-range MEMS lidar can detect a low reflectance target at 130 m under the bright daylight while it has a narrow FoV of 10 deg × 11 deg and equips an MEMS control application specific integrated circuit (ASIC) with a PLL for a resonant MEMS mirror to ensure stable and robust operation. A vibration test setup is developed for the lidar by subjecting the transmitter module to vibrations. Using the vibration test setup, the benefits of the PLL for resonant MEMS mirrors are verified under a wideband vibration based on the automotive standard LV124,[21] demonstrating stable point cloud measurements for indoor and outdoor scenes by two quality measures.

The rest of the paper is organized as follows. Section 2 describes the long-range 1D MEMS lidar and the MEMS control ASIC used in this paper. The vibration test setup is illustrated in Sec. 3 to test the vibration influence on the lidar measurements. In Sec. 4, experimental results of lidar measurements are discussed for robustness against external vibrations according to different MEMS control conditions. Finally, Sec. 5 concludes with a summary of the outcome of the paper.

2 Long-Range 1D Scanning MEMS Lidar

Figure 1 illustrates a long-range 1D scanning MEMS lidar and its schematics of the components inside. The lidar is designed for long-range detection by reducing its FoV, where the horizontal

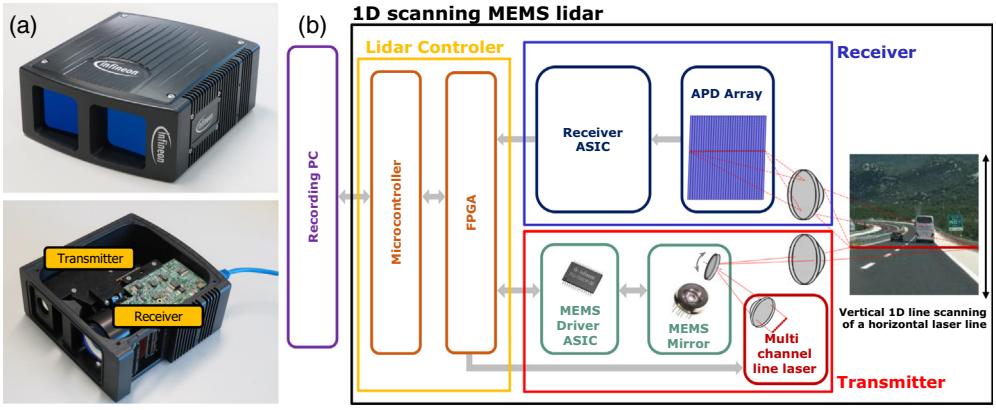

Fig. 1 (a) Picture of the 1D scanning MEMS lidar and its opened box, showing locations of the transmitter and the receiver and (b) schematics of the 1D scanning MEMS lidar with signal flow between components.

and vertical FoV are set to 10 deg and 11 deg, respectively, allowing detection of the use case scenario "tire on the road," e.g., a 10% of low reflectivity target at 130-m distance outdoor in bright sunlight, and covering more than four lanes in the straight highway at a distance of 100 m. The laser module generates eight lines of 905-nm wavelength within 10-ns pulses. The resonant MEMS mirror scans the laser line along the vertical axis while the horizontal pixels are produced by an avalanche photodiode (APD) array with 32 channels along the horizontal axis.[3,4,9] The number of pixels per frame is set to 32×220, corresponding to the horizontal and vertical pixel resolution of 0.31 deg $\times$0.05 deg, respectively. The frame rate is 29 Hz.

The lidar has three main function blocks: transmitter, receiver, and lidar controller. The transmitter block includes the laser module, transmitter optics, and an MEMS scanning system including an MEMS scanning mirror and its driver ASIC. The receiver block consists of receiver optics, the APD array, and receiver ASICs, which process multiple channels of the APD readouts. The lidar controller has been implemented in a field programmable gate arrays (FPGA) and a microcontroller. The digital system in the FPGA includes the control of the laser pulse timing according to the mirror movements, time of flight calculation based on the receiver signal, and functional safety to ensure safe operation of the lidar, especially eye safety. The microcontroller has multiple cores inside, which are used for defining the starting sequence of the lidar as well as the packet generation of the point cloud measurements for data transfer to an external data recording PC via Ethernet.

Figure 2 describes the block diagram of the resonant MEMS mirror and the MEMS driver ASIC with the FGPA and the microcontroller in the lidar controller. For operation in a positive phase,[23] the mirror operates with an optical scanning angle of ± 16.5 deg while the scanning angle is scaled by one-third for designed FoV via an optical system after the MEMS mirror, also allowing a sharp optical resolution in the vertical axis. Since the optical resolution is mainly determined by the size of the mirror, this scan range scaling can be also regarded as a relaxation of a small mirror size. The resonant MEMS mirror used in the lidar is a variant of the MEMS mirrors in Refs. 9, 16, and 24. The MEMS mirror has an elliptical shape with a long axis of 2.7 mm and is actuated by out-of-plane electrostatic comb drives. The mirror features leaf springs that exhibit stiffening as the amplitude increases and also has a reinforcement structure, allowing a flat mirror surface at a high-frequency operation. The design concepts are discussed in detail in Ref. 24. The variant MEMS mirror design in the lidar improves long-term reliability for large operating amplitudes while resulting in a reduction of the resonant frequency. This cannot maintain the robustness condition of the resonant frequency over 2 kHz in Ref. 16, i.e., external vibrations defined in an automotive standard LV124 may threaten the reliable performance of the lidar measurements.

To ensure the stable and robust operation of the MEMS scanning motion, an MEMS driver ASIC is used.[9,25] The MEMS driver ASIC mainly consists of a mirror position sensor, a PLL with amplitude control, and a high-voltage (HV) driver. The mirror position sensor detects the zero crossing of the MEMS mirror and specific angle points from the displacement currents of the MEMS mirror stators i_s. Based on the mirror position measurements, the PLL calculates the errors of the amplitudes as well as the phase and regulates the mirror dynamics to provide a stable operation of the scanning frequency and amplitudes of the MEMS mirror. The PLL control is implemented digitally by the timing regulation,[22,25] and PI controllers are implemented for both

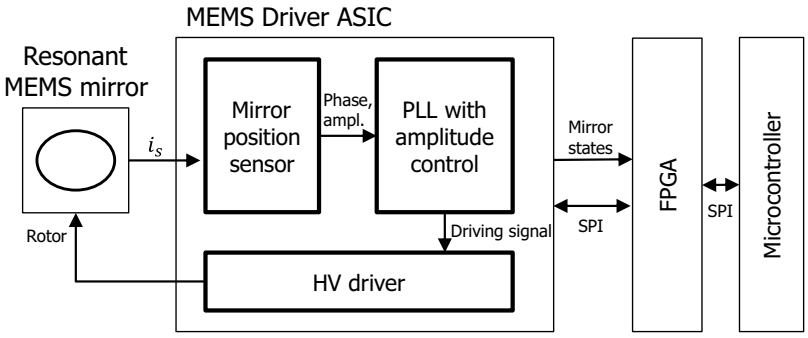

Fig. 2 Block diagram of the MEMS driver ASIC its connection to the MEMS mirror and FPGA.

phase and amplitude control, determining the driving signal of the MEMS mirror. This driving signal is amplified by the HV driver and applied to the rotor of the MEMS mirror. Further details about the MEMS driver ASIC design can be found in Ref. 25.

For the lidar operation, the MEMS driver ASIC provides the states of the MEMS mirror such as the mirror position information including scanning direction and amplitude. Based on the mirror state information and prior knowledge of the scanning trajectory, the laser control module in the FPGA generates short laser pulse signals at scheduled angles of the MEMS mirror. The channels of the laser module are scheduled for the illumination of the scene while keeping a high frame rate and laser class 1 operation. Thanks to a scanning frequency higher than the frame rate, the laser lines can be scheduled in a noncontinuous manner, providing more margin for laser safety. For the startup sequence, configuration, and monitoring of the MEMS scanning system, the microcontroller can access specific registers in the MEMS driver ASIC via the FPGA. This includes the gain configuration of the PI controllers for both the phase and the amplitude control.

3 Vibration Test Setup

Figure 3(a) illustrates the vibration test setup for the 1D scanning MEMS lidar. A shaker (TV 51110-M, Tira GmbH, Schalkau, Germany) induces the vibration to the transmitter module, which contains the laser module and transmission optics as well as the MEMS mirror. The applied vibration is measured by a laser Doppler vibrometer (OFV 534 with OFV 5000, Polytec GmbH, Waldbronn, Germany) for the regulation of the applied vibrations. The receiver and the lidar controller are fixed next to the transmitter. Only the transmitter is installed on the shaker due to a limited force to accelerate the mass for vibration tests. This is still a valid setting because the transmitter is more sensitive to the vibration by the influence to the MEMS mirror dynamics[16] than the receiver with fixed imaging optics and the APD array. Especially translational vibrations along the vertical axis would not influence the receiver much due to the long rectangular pixels along that vibration direction. The vibration is along the vertical scan direction while the mirror is tilted to the vibration about 70 deg as shown in Fig. 3(a). Since the mirror scanning frequency is 1792 Hz and the vibration influence is high near the scanning frequency,[16] a wideband random vibration with a bandwidth from 1 to 2 kHz is considered for the evaluation of vibration influences, which is with a constant power spectral density of 0.14 $(\mathrm{m/s^2})^2/\mathrm{Hz}$, as shown in Fig. 3(b), corresponding to the total root mean square (RMS) acceleration of 11.8 m/s. This vibration profile is the high-frequency part of the vibration profile D (total RMS acceleration 30.8 m/s) for hang-on parts on sprung masses in the automotive standard of LV124[21] [red dashed line in Fig. 3(b)], which is relevant for the automotive test.

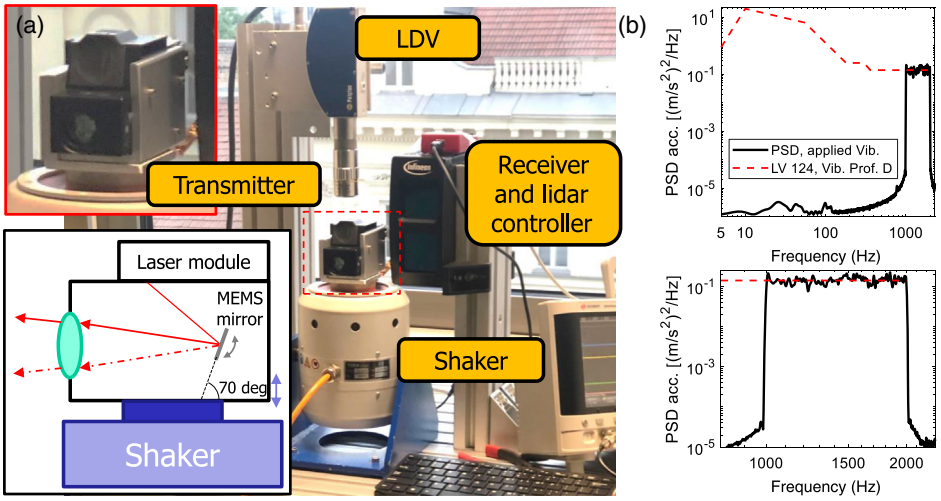

Fig. 3 (a) Vibration test setup for the 1D scanning MEMS lidar and (b) power spectral density of the applied vibration, measured by laser Doppler vibrometer.

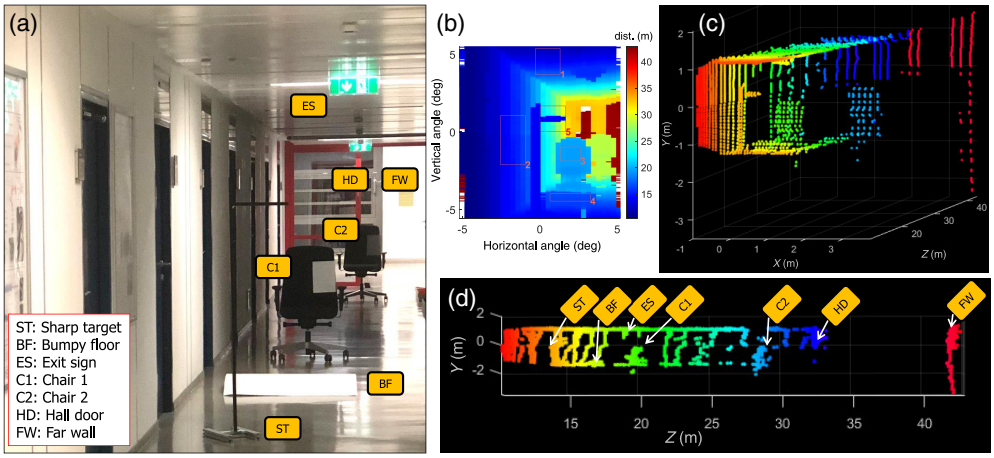

Fig. 4 (a) Picture of the indoor test scene, (b) angle-radial distance map of the indoor scene and five RoIs of the scene for quantitative evaluation, (c) point cloud of the indoor scene in perspective view, and (d) point cloud in a view along the distance.

4 Experimental Evaluation of Robustness against Vibrations

To evaluate the vibration influences to the 1D scanning MEMS lidar measurements, an indoor and an outdoor scene is considered. Figure 4(a) illustrates the indoor scene of the corridor with several features for the test such as a sharp target, a bumpy floor, and various surfaces of the walls, the floor, and the ceiling. The lidar measures the radial distance by ToF measurements, as shown in Fig. 4(b). Then the point cloud is generated by the combination of the radial distances, the scanning position, and the pixel location at the detector, as shown in Fig. 4(c). Figure 4(d) illustrates the major features along with the distance. It is readily observed that some points are below the floor or above the ceiling mainly due to the specular reflection with the shallow incident angle by the floor or the ceiling, respectively. Figure 5(a) depicts an outdoor scene, a small facade, and a rooftop of a building at a distance of over 30 m. The angle-radial distance map and point cloud generation can be drawn in the same manner. The far distance objects around 93 m are leaves of the tree, shown above the rooftop.

For evaluation, three control conditions are considered, i.e., an open loop without control, a PLL control, and a PLL control with a high gain (HG). The open loop case disables the PLL, and the PLL control case exploits the default low gain of the MEMS driver ASIC, which is chosen for a stable operation of the mirror and EMI influence. For the PLL with a HG case, all gains are increased more than two times higher than the default value. Figure 6 illustrates angle-radial distance maps and the point clouds under the wideband vibrations for three control conditions.

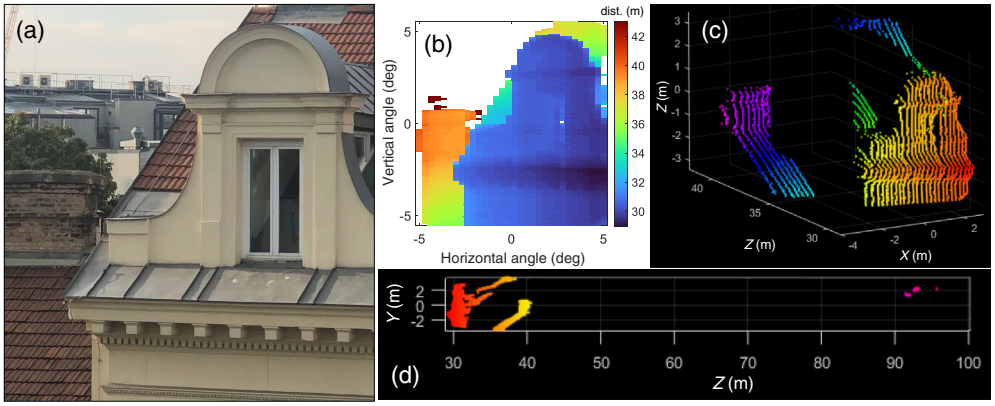

Fig. 5 (a) Picture of the outdoor test scene, (b) angle-radial distance map of the outdoor scene, (c) a point cloud of the outdoor scene in perspective view, and (d) point cloud in a view along the distance.

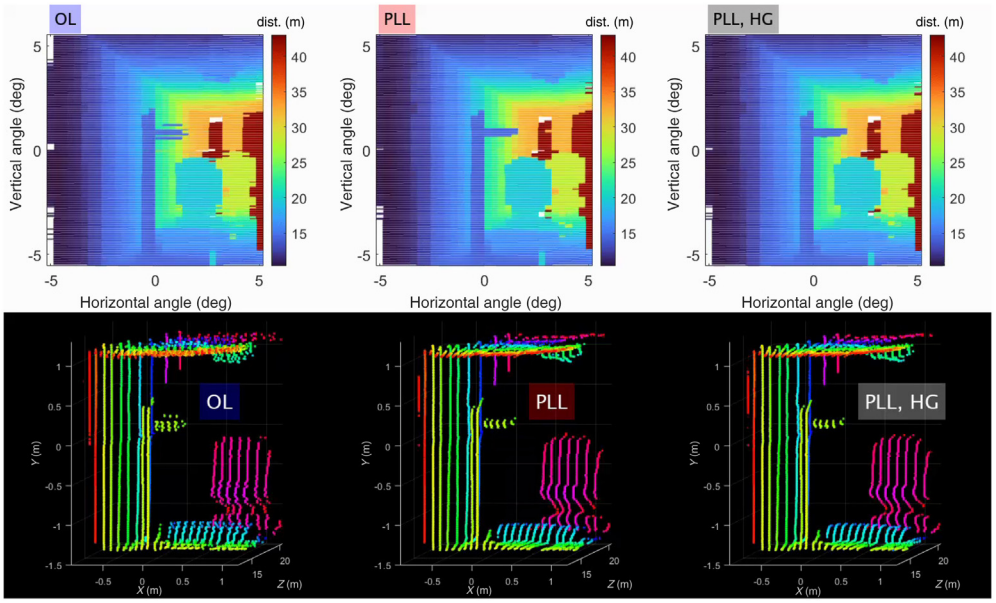

Fig. 6 Angle-radial distance maps and the point clouds nder the wideband vibration for three different control conditions of open loop (OL), PLL control (PLL), and PLL control with a high gain (PLL, HG). The videos without vibrations and the outdoor scene are also available (Video 1, MP4, 8093 KB [URL: https://doi.org/10.1117/1.JOM.2.1.011007.1]; Video 2, MP4, 8429 KB https://doi.org/10.1117/1.JOM.2.1.011007.2; Video 3, MP4, 5360 KB https://doi.org/10.1117/1.JOM.2.1.011007.3; and Video 4, MP4, 5338 KB https://doi.org/10.1117/1.JOM.2.1.011007.4).

Video 2 shows that the pixels of the radial distance are not properly measured due to the scanning position errors induced by the vibration, leading to wobbly point clouds in the open loop case. The wobbly point cloud movements are effectively suppressed by both the PLL and the PLL with a HG, which is comparable with the vibration-free case.

To evaluate this robustness performance quantitatively, quality measures are applied for point clouds at five region of interest (RoI), shown in Fig. 7(b). First of all, RoI #1, #2, #3, and #4 represent specific planes in the scene. The RoI #1 corresponds to a plane of the ceiling where radian distance varies along the vertical direction. On the contrary, RoI #2 represents a plane where the radial distance varies along the horizontal direction. RoI #3 is a plane almost perpendicular to the radial direction and RoI #4 is similar to RoI #1 but with a nonlinear plane with a curvature. For RoI #1 to #4, a standard error of point to surface in area A is given as[26]

$$E_{\mathrm{p2s,A}} = \sqrt{\frac{1}{N_{\mathrm{A}}} \sum_{i,j \in A} (\vec{e}_{i,j} \cdot \vec{n}_{\mathrm{A}})^2}, \tag{1}$$

where $\vec{e}_{i,j}$ denotes the error vector of the horizontal and vertical pixel index of i and j, respectively, and $\vec{n}_{\mathrm{A}}$ is the normal vector of the surface A, estimated by *pcfitplane* in MATLAB.[27] The error vector is calculated based on the mean radial distance of the vibration-free scene for each control condition. N_{A} denotes the number of pixels in the area. The square root makes the error in the unit of the distance, e.g., mm. This point to surface error represents the perceived quality in the surfaces structured scene while the errors tend to decrease for the surfaces with high angle to the radial direction considering the dominant radial distance errors in the lidar measurements. For the case of the sharp bar target with 20-mm thickness in RoI #5, an RMS thickness of the bar is proposed as a quality measure

$$T_{\mathrm{bar}} = \sqrt{\frac{1}{N_{\mathrm{bar}}} \sum_{i,j \in A_{\mathrm{bar}}} (y_{i,j} - y_{\mathrm{c}})^2}, \tag{2}$$

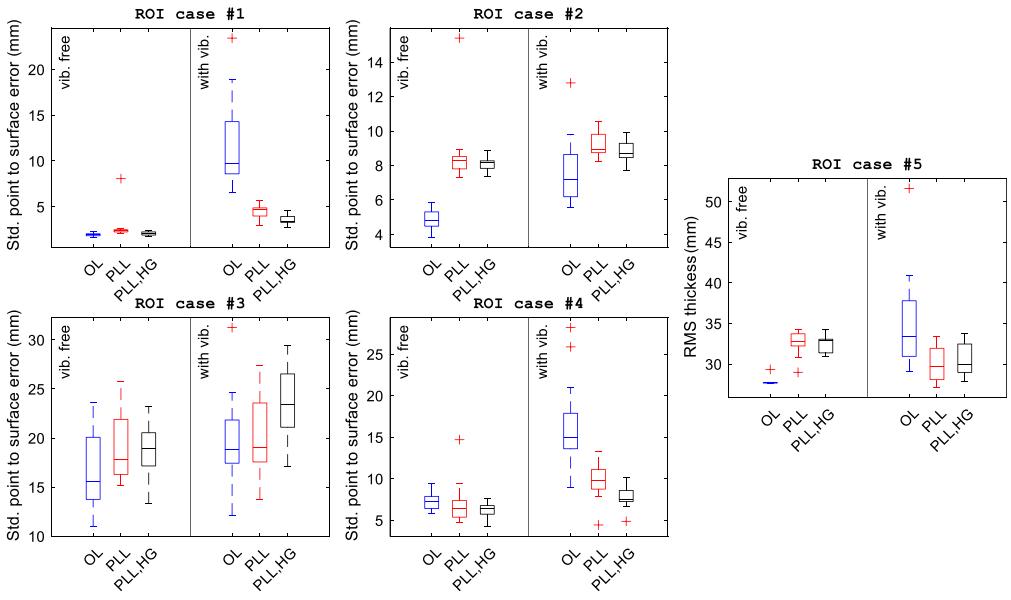

Fig. 7 Box plots of the standard point to surface errors for RoI #1 to #4 and the RMS thickness in RoI #5 for 300 frames. The evaluation of open loop (OL), PLL control (PLL), and PLL control with a high gain (PLL, HG) in case of vibration free and under the wideband vibration.

where $y_{i,j}$ denotes a vertical position of the detected pixels of the bar and y_c is the center position of the bar in the measurements. N_{bar} denotes the number of pixels on the bar in the area A_{bar}. This RMS thickness measures the deviation of the pixel position of the thin bar shape.

Figure 7 describes box plots of the standard point to surface errors and the RMS thickness for the RoIs for 300 frames. Under the wideband vibration and in the open loop case, large error increases can be measured in RoI #1 and #4 where the plane varies the radial distance by the scanning axis. For the surface of RoI #2 that varies the radial distance only orthogonal to the scan-axis and the perpendicular surface of RoI #3 shows less sensitivity to the vibration. Both the PLL and the PLL with a HG can slightly increase errors in some cases without vibrations mainly due to feedback of the sensor noise, but demonstrate improved errors under the vibration by reducing its mean value up to 69.3% and its standard deviation up to 90.0%. The PLL with a HG shows a better performance for ROI #1 and #4 than the PLL with the default low gain. The standard deviation of the RMS thickness in the open loop case increases 12.8 times larger after the vibration is applied while the PLL with a HG reduces it up to 67.4%. These results prove that a PLL control design for MEMS mirrors can improve the robustness against external vibrations, enabling stable point cloud measurements with a 1D scanning MEMS lidar even under vibrations on the scanning frequency of the MEMS mirror.

5 Conclusion

This paper discusses robustness against external vibrations for a long-range 1D scanning MEMS lidar. The 1D scanning MEMS lidar provides 10 deg and 11 deg of horizontal and vertical FoV, respectively, at 29 frames per second by scanning horizontal laser lines along the vertical axis. The MEMS mirror used in the lidar has improved long-term reliability but with reduced scanning frequency below 2 kHz, leading to a concern of the qualification against vibrations in an automotive standard LV124. An MEMS driver ASIC in the lidar includes a PLL with an amplitude control to ensure the stable and robust operation of the MEMS mirror. A vibration test setup is developed for applying a wideband vibration based on LV124 to the transmitter module of the 1D scanning MEMS lidar, which is expected to have high sensitivity to the external vibration. For vibration tests, the control conditions of an open loop without control and PLLs with two different gains are evaluated for both indoor and outdoor scenes. The measured point clouds demonstrate that the PLL in the MEMS driver ASIC can suppress the vibration influence well

for the worst ROI in the scene, reducing the mean and standard deviation of the standard point to surface errors up to 69.3% and 90.0% compared with the open loop case, respectively. The videos under the wideband vibration also show the stable point cloud with the PLL, proving the benefits of the control for MEMS mirror used in automotive-qualified MEMS lidars to achieve high robustness against external vibrations.

Acknowledgments

The authors would be grateful Infineon Technologies for generous support in providing the long-range 1D MEMS lidar for evaluation. The authors would like to thank Norbert Druml, Boris Kirillov, Stefan Mendel, Simon Achatz, and Daniel Schloms for helps to run the lidar, and Stephan Albert, Malika Bella, Thomas Thurner, Marcus Hennecke, and Marten Oldsen for fruitful discussions and support to enable this work. This work has been supported by the Austrian Research Promotion Agency (FFG) under the scope of the AUTOScan project (FFG project number 884345). The authors declare no conflicts of interest.

Data, Materials, and Code Availability

No data were generated or analyzed in the presented research.

References

1. S. Grigorescu et al., "A survey of deep learning techniques for autonomous driving," *J. Field Rob.* **37**(3), 362–386 (2020).
2. Y. Li and J. Ibanez-Guzman, "Lidar for autonomous driving: the principles, challenges, and trends for automotive lidar and perception systems," *IEEE Signal Process. Mag.* **37**, 50–61 (2020).
3. R. Thakur, "Scanning LIDAR in advanced driver assistance systems and beyond: building a road map for next-generation LIDAR technology," *IEEE Consum. Electron. Mag.* **5**, 48–54 (2016).
4. H. W. Yoo et al., "MEMS-based lidar for autonomous driving," *Elektrotech. Inftech.* **135**, 408–415 (2018).
5. K. Ito et al., "System design and performance characterization of a MEMS-based laser scanning time-of-flight sensor based on a 256 × 64-pixel single-photon imager," *IEEE Photonics J.* **5**, 6800114 (2013).
6. U. Hofmann et al., "Resonant biaxial 7-mm MEMS mirror for omnidirectional scanning," *JM3* **13**, 011103 (2013).
7. G. Kim and Y. Park, "LIDAR pulse coding for high resolution range imaging at improved refresh rate," *Opt. Express* **24**, 23810–23828 (2016).
8. B. L. Stann, J. F. Dammann, and M. M. Giza, "Progress on MEMS-scanned ladar," *Proc. SPIE* **9832**, 98320L (2016).
9. N. Druml et al., "1D MEMS micro-scanning LiDAR," in *Int. Conf. Sens. Device Technol. and Appl.*, pp. 48–53 (2018).
10. T. Sandner et al., "Hybrid assembled MEMS scanner array with large aperture for fast scanning LIDAR systems," *Tech. Mess.* **86**, 151–163 (2019).
11. A. Kasturi et al., "Comparison of MEMS mirror LiDAR architectures," *Proc. SPIE* **11293**, 112930B (2020).
12. F. Schwarz et al., "Resonant 1D MEMS mirror with a total optical scan angle of 180° for automotive LiDAR," *Proc. SPIE* **11293**, 1129309 (2020).
13. J.-Y. Hwang, J.-U. Bu, and C.-H. Ji, "Low power electromagnetic scanning micromirror for LiDAR system," *IEEE Sens. J.* **21**, 7358–7366 (2021).
14. J. Wang, G. Zhang, and Z. You, "Design rules for dense and rapid Lissajous scanning," *Microsyst. Nanoeng.* **6**, 101 (2020).
15. A. Wolter et al., "Applications and requirements for MEMS scanner mirrors," *Proc. SPIE* **5719**, 64–76 (2005).

16. H. W. Yoo et al., "Experimental evaluation of vibration influence on a resonant MEMS scanning system for automotive lidars," *IEEE Trans. Ind. Electron.* **69**, 3099–3108 (2021).
17. I. Maksymova et al., "Adaptive MEMS mirror control for reliable automotive driving assistance applications," in *23rd Euromicro Conf. Digital Syst. Design (DSD)*, pp. 469–475 (2020).
18. J. Grahmann et al., "Vibration analysis of micro mirrors for LIDAR using on-chip piezoresistive sensor," *Proc. SPIE* **11293**, 1129308 (2020).
19. Y. Hua et al., "Dynamic modeling and anti-disturbing control of an electromagnetic MEMS torsional micromirror considering external vibrations in vehicular LiDAR," *Micromachines* **12**, 69 (2021).
20. N. Boni et al., "Quasi-static PZT actuated MEMS mirror with 4×3 mm^2 reflective area and high robustness," *Proc. SPIE* **11697**, 1169708 (2021).
21. "LV 124: electric and electronic components in motor vehicles up to 3.5 t – general requirements, test conditions and tests (VW 80000)," Tech. Rep. 8MA00, Volkswagen (2013).
22. D. Brunner, H. W. Yoo, and G. Schitter, "Linear modeling and control of comb-actuated resonant MEMS mirror with nonlinear dynamics," *IEEE Trans. Ind. Electron.* **68**, 3315–3323 (2021).
23. H. W. Yoo, S. Albert, and G. Schitter, "Fourier series-based analytic model of a resonant MEMS mirror for general voltage inputs," *J. Microelectromech. Syst.* **30**, 343–359 (2021).
24. H. W. Yoo, S. Albert, and G. Schitter, "Accurate analytic model of a parametrically driven resonant MEMS mirror with a Fourier series-based torque approximation," *J. Microelectromech. Syst.* **29**, 1431–1442 (2020).
25. I. Maksymova et al., "A MEMS mirror driver ASIC for beam-steering in scanning MEMS-based LiDAR," *Proc. SPIE* **11107**, 111070C (2019).
26. D. Tian et al., "Geometric distortion metrics for point cloud compression," in *IEEE Int. Conf. Image Process. (ICIP)*, pp. 3460–3464 (2017).
27. P. H. S. Torr and A. Zisserman, "MLESAC: a new robust estimator with application to estimating image geometry," *Comput. Vision Image Understanding* **78**, 138–156 (2000).

Han Woong Yoo is a postdoctoral researcher in Advanced Mechatronic Systems at the Automation and Control Institute (ACIN) of TU Wien. He received his BSc degree from Yonsei University and his MSc degree from Seoul National University, and his PhD from Delft University of Technology in 2005, 2007, and 2015, respectively. He worked at Samsung Advanced Institute of Technology and Samsung Electronics Co. Ltd. for digital RF and multilevel nonvolatile memories. His main research interests are optical metrology, precision mechatronics systems, and biomedical imaging.

David Brunner is a PhD student in advanced mechatronic systems at the Automation and Control Institute (ACIN) of TU Wien and currently working on MEMS-based laser beam scanning at Infineon Technologies Austria AG. He received his MSc degree in energy systems and automation technology from TU Wien, Austria, in 2017. His primary interests include advanced identification and control concepts, high-performance mechatronic systems, and system integration.

Matthias Macho is a master's student at the Automation and Control Institute (ACIN) of TU Wien. He received his BSc degree in energy systems and automation technology from TU Wien, Austria, in 2019. His current interest is control concepts for MEMS mirrors.

Leonhard Niedermueller is a verification engineer of the Component Verification Group at Infineon Technologies Austria AG in Graz, Austria. He studied at the Technical University Graz. His current research interests are micro-electro-mechanical systems (MEMS) and their different possible applications as sensors, like pressure, gas, and the application of optical beam steering with MEMS.

Angel Jurado Devesa is a concept engineer at Infineon Technologies Austria AG in Graz, Austria, and a PhD student at Technical University of Graz. He received his BS degree in electronic and automatic industrial engineering from Universidad de Alcalá de Henares, Spain, and

MS degree in FH Joanneum, Austria. His current interests are autmotive sensors such as radar and lidar.

Leonhard Kormann is a principal engineer for component verification at Infineon Technologies Austria AG in Graz. He received his BS and MS degrees in telematics from the Technical University of Graz 2003 and 2005, respectively. His current research interests include high performance optical scan systems, optical metrology, and projection technology.

Georg Schitter is a professor for advanced mechatronic systems at the Automation and Control Institute (ACIN) of TU Wien. He received his MSc degree in electrical engineering from TU Graz, Austria, in 2000 and his MSc and PhD degrees from ETH Zurich, Switzerland, in 2004. His primary research interests are on high-performance mechatronic systems for applications in the high-tech industry, scientific instrumentation, and mechatronic imaging systems, such as AFM, scanning laser and LIDAR systems, telescope systems, adaptive optics, and lithography systems.